Transport and thermal behavior of the charge density wave phase transition in CuTe

C. N. Kuo,[1] R. Y. Huang,[2] Y. K. Kuo,[2,*] and C. S. Lue[1,†]
[1]*Department of Physics, National Cheng Kung University, Tainan 70101, Taiwan*
[2]*Department of Physics, National Dong Hwa University, Hualien 97401, Taiwan*

(Received 8 September 2020; accepted 12 October 2020; published 23 October 2020)

Copper monotelluride CuTe is of current interest due to the discovery of the quasi-one dimensional charge density wave (CDW) behavior below the transition temperature $T_{CDW} \simeq 335$ K. To explore the transport and thermodynamic properties and provide experimental insights into the underlying origins of the CDW, we have carried out a combined study by means of the electrical resistivity, Seebeck coefficient, thermal conductivity, as well as specific heat measurements on single crystalline CuTe. The CDW phase transition has been characterized by marked features near T_{CDW} from all measured physical quantities. In particular, the observed Seebeck coefficient and electronic thermal conductivity exhibit a pronounced reduction as cooling the temperature across T_{CDW}, indicative of the partially gapped Fermi surfaces associated with the CDW formation. From the examination of the excess specific heat in the vicinity of T_{CDW}, we obtained evidence for the strong-coupling character of the CDW, suggesting that the electron-phonon coupling plays an important role for the CDW instability in CuTe.

DOI: 10.1103/PhysRevB.102.155137

I. INTRODUCTION

Binary compound of CuTe has been reported to be a unique charge density wave (CDW) system with the transition temperature at $T_{CDW} \simeq 335$ K [1]. The CDW-type modulation along the wave vector $q_{CDW} = (0.4, 0.0, 0.5)$ has been identified by the analysis of the superlattice in the diffraction images of the high-resolution transmission electron microscopy (HRTEM) [2]. This observation coincides with the electronic band nesting wave vector obtained from the angle-resolved photoemission spectroscopy (ARPES) experiment [1]. Based on the peak feature of the computed electronic susceptibility, the Fermi-surface nesting driven by the electron-electron scattering has been proposed to be responsible for the CDW ordering [1]. In addition, the calculated phonon dispersion showing a softening mode at $q_{ph} = (0.4, 0.0, 0.5)$ is identical with the direction of the CDW modulation. With this accordance, the electron-phonon coupling would be a possible origin for the CDW instability [1]. Very recently, a theoretical calculation further revealed the emergence of the imaginary phonon frequency at q_{ph} as including the Coulomb correction of Cu d electrons [3]. Such a result highlights the importance of the interplay between electron-electron correlation and the electron-phonon interaction for the CDW in CuTe.

While CuTe adopts an orthorhombic structure [2,4], the aforementioned CDW is localized on the chain of the Te atoms separated by the wrinkled Cu layer [1,2], making CuTe a quasi-one-dimensional (1D) character of the CDW. Among the reported quasi-1D CDW compounds, $NbSe_3$ and $K_{0.3}MoO_3$ are well-studied examples. The thermodynamic properties related to the CDW phase transition for both materials have been widely investigated since the thermodynamic parameters could be affected by the critical fluctuations arising from the interchain coupling [5–12]. As motivated, it is desirable to examine whether CuTe follows similar thermodynamic behavior as in conventional quasi-1D CDWs. Moreover, the characterization of thermodynamic features in CuTe, especially focusing on the temperature region in the vicinity of T_{CDW}, would be essential to elucidate the nature of the CDW transition. Nevertheless, thermal properties of CuTe have not been explored to the best of our knowledge.

In order to provide experimental insights into the thermodynamic properties and the CDW phase transition, we have carried out a combined study of single-crystalline CuTe by means of the electrical resistivity, Seebeck coefficient, thermal conductivity, as well as specific-heat measurements. Distinctive features associated with the CDW transition near $T_{CDW} \simeq 335$ K have been observed by all measured thermodynamic quantities. The lack of the thermal hysteresis behavior indicates the second-order phase transition in nature. The pronounced reductions in the Seebeck coefficient and electronic thermal conductivity across T_{CDW} give indications for the partially gapped Fermi surfaces. From the analysis of the excess specific heat in the vicinity of T_{CDW}, we obtained conclusive evidence for the strong-coupling character of the CDW, suggesting that the electron-phonon coupling plays an essential role for the CDW instability in CuTe.

II. EXPERIMENT DETAILS

Single crystals of CuTe were grown by a Te self-flux method. The high-purity elements of Cu (99.99%) and Te (99.9999%) were mixed with a molar ratio of 35:65. The

*Corresponding author: ykkuo@gms.ndhu.edu.tw
†Corresponding author: cslue@mail.ncku.edu.tw

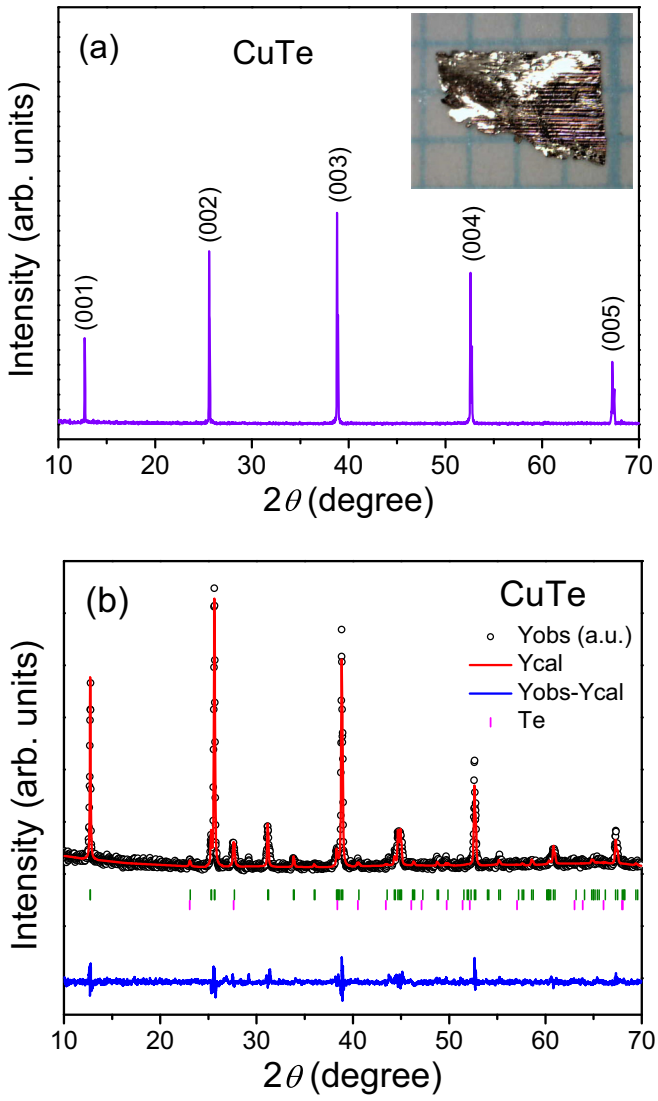

FIG. 1. (a) Single-crystal x-ray diffraction of the (00l) planes measured at room temperature. The inset shows a photograph of CuTe crystal. (b) Room-temperature powder XRD pattern with the Rietveld refinement for crushed single crystals of CuTe, in which all diffraction peaks can be indexed to *Pmmn* space group. The black cross and red and blue lines represent the observed pattern, calculated profile, and the difference between the observed and calculated intensities, respectively.

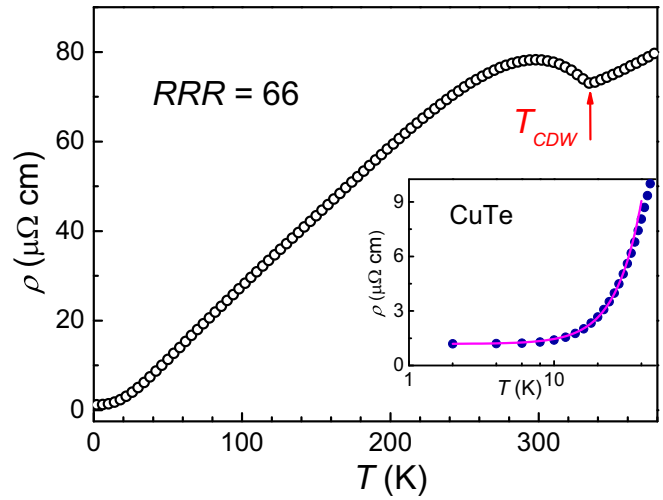

FIG. 2. Temperature variation of the electrical resistivity ρ of CuTe. The arrow indicates the temperature of T_{CDW}. Inset: The data of ρ below 50 K with a solid curve which are a fit to a power law described in the text.

mixture was transferred to a fused quartz tube and sealed under vacuum. The quartz tube was heated up to 600 °C for 10 h, cooled to 430 °C for 2 h, and then slowly cooled down to 350 °C at a rate of 1 °C/h. The excess flux was decanted with a centrifuge at 350 °C and several plateletlike crystals with a typical size of $2 \times 3 \times 0.2\,\mathrm{mm}^3$ were mechanically removed from the inner wall of the quartz tube. A photograph of single-crystalline CuTe is given in the inset of Fig. 1(a). The single-crystal x-ray diffraction (XRD) pattern is shown in Fig. 1(a). Only sharp (00l) diffraction peaks are observable, suggesting that the crystallographic c axis is perfectly perpendicular to the surface facet of the crystal. We also performed XRD on a powder specimen which was obtained by crushing several single crystals. As displayed in Fig. 1(b), all diffraction peaks can be indexed to the expected *Pmmn* space group. The Rietveld refinement for the room-temperature XRD patterns yields the lattice parameters $a = 3.149 \pm 0.002$, $b = 4.085 \pm 0.002$, and $c = 6.951 \pm 0.004$ Å, identical with those reported in the literature [1,2,4].

Electrical resistivity was measured using a standard four-probe method, with an electrical current flowing along the direction perpendicular to the c axis of the crystal. The Seebeck coefficient and thermal conductivity measurements were performed in a closed-cycle refrigerator, using a direct heat-pulse technique. The temperature difference was detected by an E-type differential thermocouple with junctions thermally attached to two well-separated positions along the longest direction of the specimen. The low-temperature specific-heat measurement was carried out in a physical property measurement system (PPMS) with a heat-pulsed thermal relaxation calorimeter in the temperature range from 0.2 to 3.8 K. The high-temperature specific-heat data between 85 and 400 K were obtained from a home-built ac calorimeter, using chopped light as a heat source.

III. RESULTS AND DISCUSION

Temperature dependence of the electric resistivity ρ for CuTe is displayed in Fig. 2. At low temperatures, ρ tends to be a constant, with a small residual resistivity $\rho_o = 1.19\,\mu\Omega\,\mathrm{cm}$ at $T = 2\,\mathrm{K}$, yielding a large residual resistivity ratio (RRR) $\rho(300\,\mathrm{K})/\rho(2\,\mathrm{K}) \simeq 66$. Such a result confirms the high quality of our CuTe single crystal since the residual resistivity usually arises from the scattering due to domain boundaries and/or defects. The CDW ordering is characterized by a pronounced hump near $T_{\mathrm{CDW}} \simeq 335\,\mathrm{K}$, identical with that observed by Zhang *et al.* [1]. The anomaly in ρ is a typical signature for the CDW transition attributed due to the partial opening of the electronic gap at the Fermi surfaces. Similar observations have been found in many CDW systems, e.g., $R_2\mathrm{Ir}_3\mathrm{Si}_5$ [13–17], $R\mathrm{NiC}_2$ (R = rare-earth elements) [18–27],

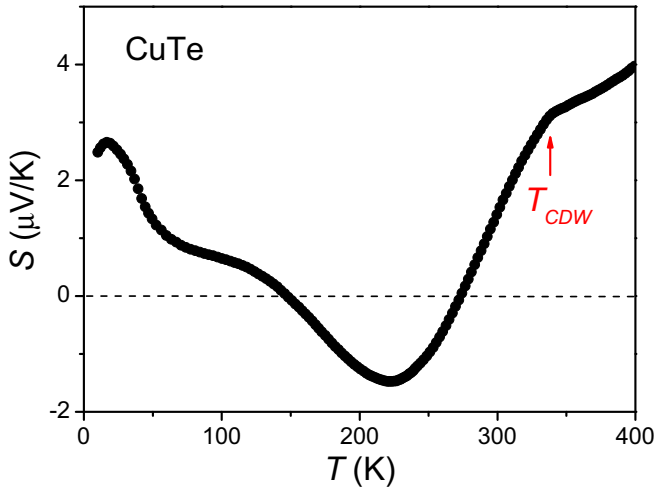

FIG. 3. Temperature dependence of the Seebeck coefficient S of CuTe. The arrow indicates the position of T_{CDW}.

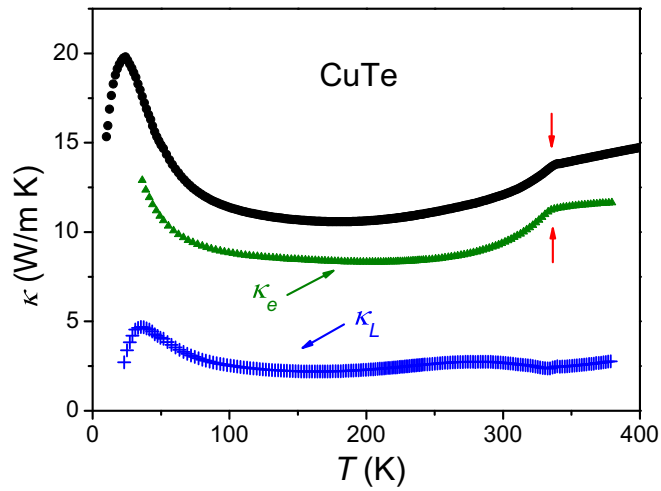

FIG. 4. Temperature variation of the thermal conductivity κ of CuTe. The dotted and cross curves represent the decomposed electronic and lattice thermal conductivity, respectively. The arrows highlight the temperature of T_{CDW}.

$LaAgSb_2$ [28–30], and $LuPt_2In$ [31]. Below 30 K, ρ can be fitted to the power-law relation $\rho = \rho_0 + AT^n$, as shown in the inset of Fig. 2. The prefactor $A \sim 1 \times 10^{-3}\,\mu\Omega\,\mathrm{cm\,K}^{-n}$ with the exponent $n = 2.43$ was extracted from the fit. The obtained exponent n falling in between 2 and 3 has also been reported in other quasi-1D materials [32–34], presumably attributed to the electron-electron umklapp scattering at low temperatures [35].

It is known that the Seebeck coefficient is a sensitive probe for the phenomenon associated with changes in the Fermi surfaces, such as CDW ordering and structural distortions [17,21,29,36–44]. As shown in Fig. 3, the observed S exhibits a strong temperature dependence, indicative of the multiband effect on the thermoelectric transport in CuTe. Accordingly, the measured Seebeck coefficient can be described as $S = (\sigma_n S_n + \sigma_p S_p)/(\sigma_n + \sigma_p)$, where $S_{n,p}$ and $\sigma_{n,p}$ represent the Seebeck coefficients and electrical conductivities for the n- and p-type carriers from electronic and hole bands, respectively. In principle, each parameter is governed by the corresponding effective mass and temperature-dependent scattering relaxation rate. According to the theoretical band calculation of CuTe, the p-type carriers are mainly from the Cu orbitals, while the n-type carriers are from the Te states [3]. Hence, the p-type carriers are dominant at high temperatures, and the sign of S is positive. With lowering the temperature, S gradually decreases and exhibits an abrupt drop in the vicinity of T_{CDW}. Upon further cooling, the contribution from the n-type carriers becomes important, leading to a sign reversal at 270 K and a presence of a broad minimum near 220 K. Below 150 K, S shows positive again, attributed to the positive phonon drag effect which peaks at around 20 K.

As for the dramatic reduction in S near T_{CDW}, it can be realized as a decrease in the number of p-type carriers due to an imbalance charge contribution arising from the modification of the Fermi surfaces. This is consistent with the theoretical band calculation, in which the reduction of the weight of Cu orbitals arising from a non-negligible Coulomb correlation has an effect to enhance the Te character at the Fermi level, leading to the enhancement of the quasi-1D nature for the CDW formation [3]. The scenario connected to the change in the electronic bands also agrees with the conclusion drawn from the results of the ARPES where an anisotropic CDW gap has been observed, suggesting the presence of the Fermi surface nesting in CuTe. It is worthwhile mentioning that similar features in S have been reported in prototypical CDW systems such as $Lu_2Ir_3Si_5$ and $LaAgSb_2$ [14,29]. In these materials, the CDW ordering associated with the Fermi surface nesting has been identified through various measurements.

Figure 4 illustrates the temperature variation of the thermal conductivity κ for CuTe. A phonon drag peak at around 20 K is identical with that found in S. Near T_{CDW}, a pronounced change has been observed, being consistent with the results of ρ and S measurements. In ordinary metals or semimetals, the total thermal conductivity is a sum of electronic and lattice contributions. The electronic thermal conductivity (κ_e) can be evaluated using the Wiedemann-Franz law: $\kappa_e \rho/T = L_0$ where ρ is the dc electrical resistivity and $L_0 = 2.45 \times 10^{-8}\,\mathrm{W\,\Omega\,K}^{-2}$ is the theoretical Lorentz number. The determined κ_e for CuTe is plotted as a dotted curve in Fig. 4. The lattice thermal conductivity κ_L, obtained by subtracting κ_e from the measured κ, is also presented in Fig. 4. It is clear that κ_e exhibits a marked drop at T_{CDW}, and the reduction feature is almost identical with the observed κ. In this respect, the decrease in κ_e across T_{CDW} implies that the CDW instability in CuTe is essentially caused by the reduction of the electronic contribution. Such an interpretation is in agreement with the description for the Fermi surface nesting associated with the CDW phase transition. Similar analyses of κ_e have been employed in various CDW materials such as $SmNiC_2$, $Rb_{0.3}MoO_3$, and $LaPt_2Si_2$ [21,45–47], for providing insights into the electronic origin for the CDW formation.

The low-temperature specific heat C_p measured between 0.2 and 3.8 K is shown in Fig. 5. The temperature dependence of C_p for CuTe exhibits a smooth increase with no signature of the magnetic or superconducting phase transition. For nonmagnetic metals at low temperatures, the experimen-

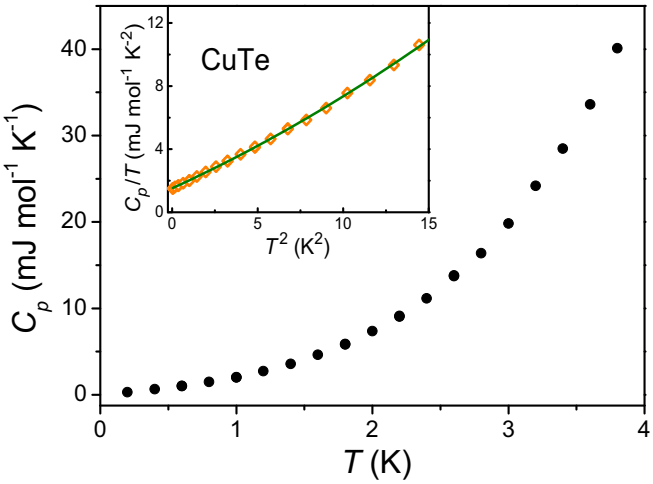

FIG. 5. Temperature dependence of the specific heat C_p of CuTe. The inset is a plot of C_p/T vs T^2 with a solid curve, which is a fit to the experimental data according to $C_p/T = \gamma + \beta T^2 + \delta T^4$ between 0.2 and 3.8 K.

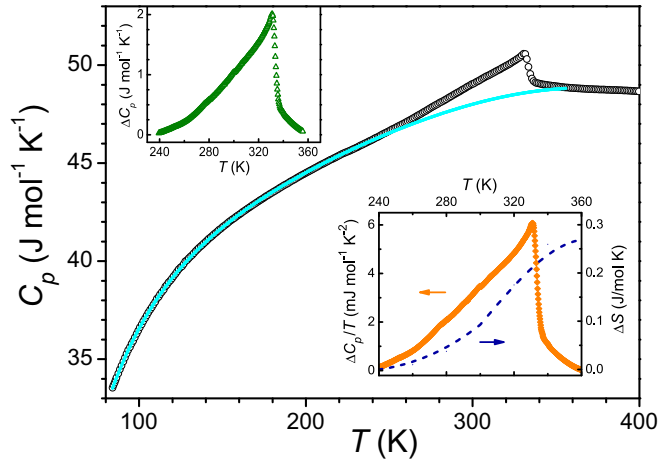

FIG. 6. Temperature-dependent C_p of CuTe over the temperature range between 85 and 400 K. The light blue curve is the calculated background due to the lattice specific heat. The upper panel of the inset is the excess specific heat ΔC_p. The lower panel of the inset shows the plot of $\Delta C_p/T$ vs T and the corresponding entropy change ΔS associated with the phase transition.

tal specific heat can be expressed as $C_p(T) = \gamma T + \beta T^3 + \delta T^5$. The first term is the electronic specific heat associated with the Sommerfeld coefficient γ while the remaining two terms arise from the contributions of the phonons including the anharmonic effect. In the inset of Fig. 5, we plotted C_p/T versus T^2, with a solid curve representing the best fit to the experimental data. Such a fit yields the values of $\gamma = 1.52\,\text{mJ mol}^{-1}\,\text{K}^{-2}$, $\beta = 0.496\,\text{mJ mol}^{-1}\,\text{K}^{-4}$, and $\delta = 0.0088\,\text{mJ mol}^{-1}\,\text{K}^{-6}$. The Debye temperature $\Theta_D = 198\,\text{K}$ was derived from β using $\Theta_D = (12\pi^4 ZR/5\beta)^{1/3}$, where $Z = 2$ is the number of atoms per formula unit and $R = 8.314\,\text{J mol}^{-1}\,\text{K}^{-1}$ is the gas constant. According to the Sommerfeld theory of conduction, the measured γ can be used to estimate the Fermi-level density of states (DOS) $N(\varepsilon_F)$ via $\gamma = (\pi^2/3)k_B{}^2 N(\varepsilon_F)$, where k_B is the Boltzmann constant and ε_F is the Fermi energy. Accordingly, a small $N(\varepsilon_F) = 0.65$ states/eV in CuTe was deduced. Such a low $N(\varepsilon_F)$ has been found to be consistent with the theoretical results obtained from different calculations [3,4]. It should be noted that this value represents an upper limit since the effect of the electron-phonon coupling was not considered here. In general, the electron-phonon coupling constant should be included to relate to the experimental γ, and consequently to reduce the value of $N(\varepsilon_F)$.

The high-temperature C_p for CuTe measured between 85 and 400 K is given in Fig. 6. The presence of an evident peak in C_p demonstrates the intrinsic phase transition at $T_{\text{CDW}} \simeq 335\,\text{K}$. We have carried out the measurement under the cooling and warming processes, and found no thermal hysteresis behavior around T_{CDW}. The absence of thermal hysteresis indicates that this phase transition is second order in nature. To gain insights into the CDW phase transition, we analyzed the excess specific heat ΔC_p in the vicinity of the phase transition. The temperature-dependent ΔC_p was obtained by subtracting a smooth background of the lattice specific heat, which was estimated by fitting the experimental data far from the transition region to a polynomial function. The result is shown in the upper inset of Fig. 6. We found $\Delta C_p/C_p \simeq 0.04$ at T_{CDW}, similar to $\simeq 0.025$ at higher $T_{\text{CDW}} \simeq 145\,\text{K}$ in $NbSe_3$ and $\simeq 0.03$ in $K_{0.3}MoO_3$ [5,48]. To further evaluate the change of the entropy ΔS associated with the CDW transition, we first determined the temperature dependence of $\Delta C_p/T$ (plotted in the lower inset of Fig. 6), and then integrated $\Delta C_p/T$ through the entire phase-transition region. The magnitude of $\Delta S \simeq 0.27\,\text{J/mol K}$ for CuTe was thus obtained. The weak anomaly of ΔC_p leading to a small entropy change is also identical with $\Delta S \simeq 0.083$ and $\simeq 0.10\,\text{J/mol K}$ for $NbSe_3$ and $K_{0.3}MoO_3$, respectively [5,48].

It is noticeable that the feature of ΔC_p in CuTe is quite different from those found in the well-characterized $Lu_5Ir_4Si_{10}$ and newly discovered $Sm_2Ru_3Ge_5$ CDW systems [49–52]. The specific heat for each of these materials exhibits a spiky cusp within a very narrow transition regime. The divergence-like ΔC_p in $Lu_5Ir_4Si_{10}$ has been attributed to the strong critical fluctuations in addition to the mean-field contribution. The origin for the critical fluctuations has been connected to the strong coupling between the quasi-1D CDW chains [50]. As viewed from the wide transition region of about 100 K, we considered that the presence of strong critical fluctuations is not likely for CuTe. In this accordance, there would be little effect on ΔC_p from the critical fluctuations but the mean-field contribution needs to be examined.

From the mean-field prediction within the weak-coupling limit [53], the specific-heat jump at the transition temperature can be expressed as $\Delta C_{\text{MF}} = 1.43\,\gamma T_{\text{MF}}$, where γ is the electronic specific-heat coefficient and T_{MF} is the mean-field temperature. Using experimental $\gamma = 1.52\,\text{mJ mol}^{-1}\,\text{K}^{-2}$ and taking $T_{\text{MF}} = 335\,\text{K}$, we evaluated $\Delta C_{\text{MF}} = 0.73\,\text{J mol}^{-1}\,\text{K}^{-1}$, much lower than the observed ΔC_p of approximately $2\,\text{J mol}^{-1}\,\text{K}^{-1}$. It thus yields an enhanced ratio of $\Delta C_p/\Delta C_{\text{MF}} = 2.74$. Such an enhancement is consistent with the high ratio of the CDW gap ($\Delta_{\text{CDW}} \simeq 0.19\,\text{eV}$) relative to $k_B T_{\text{CDW}}$ obtained from the ARPES study

[1]. Accordingly, the obtained ratio of $2\Delta_{CDW}/k_BT_{CDW} \simeq 13$ is well above the value of 3.52 in the limit of weak electron-phonon coupling [54], giving an enhanced factor of about 3.69, a bit larger than 2.74 derived here. While both values differ, the enhancement beyond the mean-field prediction implies that the effect of the electron-phonon coupling is non-negligible for the CDW phase transition in CuTe. With respect to these results, it allows us to reinforce the conclusion that the strong electron-phonon coupling plays a significant role on the CDW instability in CuTe.

IV. CONCLUSIONS

In summary, the second-order CDW phase transition in CuTe with distinctive features near $T_{CDW} \simeq 335$ K has been explored. The pronounced decrease in both S and κ at around T_{CDW} implies that the CDW ordering is essentially caused by the reduction in the number of the electronic carriers, identical with the picture of the Fermi-surface nesting associated with the CDW formation. Meanwhile, we pointed out the strong-coupling nature of the CDW, as suggested by the observed excess specific heat larger than the mean-field expectation at T_{CDW}. These results provide experimental evidence for the importance of the interplay between electron-electron correlation and the electron-phonon interaction for the CDW instability in CuTe, which was proposed by theoretical investigations.

ACKNOWLEDGMENT

This work was supported by the Ministry of Science and Technology of Taiwan under Grants No. MOST-109-2112-M-006-013-MY3 (C.SL.) and No. MOST-109-2112-M-259-007-MY3 (Y.K.K.).

[1] K. Zhang, X. Liu, H. Zhang, K. Deng, M. Yan, W. Yao, M. Zheng, E. F. Schwier, K. Shimada, J. D. Denlinger, Y. Wu, W. Duan, and S. Zhou, Phys. Rev. Lett. **121**, 206402 (2018).
[2] K. Stolze, A. Isaeva, F. Nitsche, U. Burkhardt, H. Lichte, D. Wolf, and T. Doert, Angew. Chem. Int. Ed. **52**, 862 (2013).
[3] S. Kim, B. Kim, and K. Kim, Phys. Rev. B **100**, 054112 (2019).
[4] S. Seong, T. A. Albright, X. Zhang, and M. Kanatzidis, J. Am. Chem. Soc. **116**, 7287 (1994).
[5] S. Tomic, K. Biljaković, D. Djurek, J. R. Cooper, P. Monceau, and A. Meerschaut, Solid State Commun. **38**, 109 (1981).
[6] R. S. Lear, M. J. Skove, E. P. Stillwell, and J. W. Brill, Phys. Rev. B **29**, 5656 (1984).
[7] D. Maclean and M. H. Jericho, Phys. Rev. B **47**, 16169 (1993).
[8] D. C. Johnston, Phys. Rev. Lett. **52**, 2049 (1984).
[9] S. M. DeLand and G. Mozurkewich, Solid State Commun. **72**, 245 (1989).
[10] R. S. Kwok and S. E. Brown, Phys. Rev. Lett. **63**895 (1989).
[11] R. S. Kwok, G. Gruner, and S. E. Brown, Phys. Rev. Lett. **65**, 365 (1990).
[12] J. W. Brill, M. Chung, Y.-K. Kuo, X. Zhan, E. Figueroa, and G. Mozurkewich, Phys. Rev. Lett. **74**, 1182 (1995).
[13] Y. Singh, D. Pal, S. Ramakrishnan, A. M. Awasthi, and S. K. Malik, Phys. Rev. B **71**, 045109 (2005).
[14] Y.-K. Kuo, K. M. Sivakumar, T. H. Su, and C. S. Lue, Phys. Rev. B **74**, 045115 (2006).
[15] N. S. Sangeetha, A. Thamizhavel, C. V. Tomy, S. Basu, A. M. Awasthi, S. Ramakrishnan, and D. Pal, Phys. Rev. B **86**, 024524 (2012).
[16] N. S. Sangeetha, A. Thamizhavel, C. V. Tomy, S. Basu, A. M. Awasthi, P. Rajak, S. Bhattacharyya, S. Ramakrishnan, and D. Pal, Phys. Rev. B **91**, 205131 (2015).
[17] C. N. Kuo, C. J. Hsu, C. W. Tseng, W. T. Chen, S. Y. Lin, W. Z. Liu, Y. K. Kuo, and C. S. Lue, Phys. Rev. B **101**, 155140 (2020).
[18] M. Murase, A. Tobo, H. Onodera, Y. Hirano, T. Hosaka, S. Shimomura, and N. Wakabayashi, J. Phys. Soc. Jpn. **73**, 2790 (2004).
[19] S. Shimomura, C. Hayashi, G. Asaka, N. Wakabayashi, M. Mizumaki, and H. Onodera, Phys. Rev. Lett. **102**, 076404 (2009).
[20] N. Hanasaki, Y. Nogami, M. Kakinuma, S. Shimomura, M. Kosaka, and H. Onodera, Phys. Rev. B **85**, 092402 (2012).
[21] J. H. Kim, J.-S. Rhyee, and Y. S. Kwon, Phys. Rev. B **86**, 235101 (2012).
[22] B. Woo, S. Seo, E. Park, J. H. Kim, D. Jang, T. Park, H. Lee, F. Ronning, J. D. Thompson, V. A. Sidorov, and Y. S. Kwon, Phys. Rev. B **87**, 125121 (2013).
[23] N. Yamamoto, R. Kondo, H. Maeda, and Y. Nogami, J. Phys. Soc. Jpn. **82**, 123701 (2013).
[24] H. Lei, K. Wang, and C. Petrovic, J. Phys.: Condens. Matter **29**, 075602 (2017).
[25] K. K. Kolincio, M. Roman, M. J. Winiarski, J. Strychalska-Nowak, and T. Klimczuk, Phys. Rev. B **95**, 235156 (2017).
[26] M. Roman, J. Strychalska-Nowak, T. Klimczuk, and K. K. Kolincio, Phys. Rev. B **97**, 041103(R) (2018).
[27] S. Steiner, H. Michor, O. Sologub, B. Hinterleitner, F. Hofenstock, M. Waas, E. Bauer, B. Stoger, V. Babizhetskyy, V. Levytskyy, and B. Kotur, Phys. Rev. B **97**, 205115 (2018).
[28] C. Song, J. Park, J. Koo, K.-B. Lee, J. Y. Rhee, S. L. Bud'ko, P. C. Canfield, B. N. Harmon, and A. I. Goldman, Phys. Rev. B **68**, 035113 (2003).
[29] C. S. Lue, Y. F. Tao, K. M. Sivakumar, and Y. K. Kuo, J. Phys.: Condens. Matter **19**, 406230 (2007).
[30] S. L. Bud'ko, S. A. Law, P. C. Canfield, G. D. Samolyuk, M. S. Torikachvili, and G. M. Schmiedeshoff, J. Phys.: Condens. Matter **20**, 115210 (2008).
[31] T. Gruner, D. Jang, Z. Huesges, R. Cardoso-Gil, G. H. Fecher, M. M. Koza, O. Stockert, A. P. Mackenzie, M. Brando, and C. Geibel, Nat. Phys. **13**, 967 (2017).
[32] M. H. Rashid and D. J. Sellmyer, Phys. Rev. B **29**, 2359 (1984).
[33] S. Nagata, H. Kutsuzawa, S. Ebisu, H. Yamamura, and S. Taniguchi, J. Phys. Chem. Solids **50**, 703 (1989).
[34] A. Ikhwan, U. Saleheen, R. Chapai, L. Xing, R. Nepal, D. Gong, X. Gui, W. Xie, D. P. Young, E. W. Plummer, and R. Jin, npj Quantum Mater. **5**, 53 (2020).
[35] A. Oshiyama, A. Nakao, and H. Kamimura, J. Phys. Soc. Jpn. **45**, 1136 (1978).
[36] C. S. Lue, Y.-K. Kuo, F. H. Hsu, H. H. Li, H. D. Yang, P. S. Fodor, and L. E. Wenger, Phys. Rev. B **66**, 033101 (2002).

[37] C. N. Kuo, D. Shen, B. S. Li, N. N. Quyen, W. Y. Tzeng, C. W. Luo, L. M. Wang, Y. K. Kuo, and C. S. Lue, Phys. Rev. B **99**, 235121 (2019).
[38] A. T. Burkov, T. Nakama, M. Hedo, K. Shintani, K. Yagasaki, N. Matsumoto, and S. Nagata, Phys. Rev. B **61**, 10049 (2000).
[39] C. S. Lue, H. F. Liu, S.-L. Hsu, M. W. Chu, H. Y. Liao, and Y. K. Kuo, Phys. Rev. B **85**, 205120 (2012).
[40] Y. Liu, H. Lei, K. Wang, M. Abeykoon, J. B. Warren, E. Bozin, and C. Petrovic, Phys. Rev. B **98**, 094519 (2018).
[41] C. N. Kuo, H. F. Liu, C. S. Lue, L. M. Wang, C. C. Chen, and Y. K. Kuo, Phys. Rev. B **89**, 094520 (2014).
[42] Y. Liu, W. J. Lu, D. F. Shao, L. Zu, X. C. Kan, W. H. Song, and Y. P. Sun, Europhys. Lett. **109**, 17003 (2015).
[43] C. N. Kuo, C. W. Tseng, C. M. Wang, C. Y. Wang, Y. R. Chen, L. M. Wang, C. F. Lin, K. K. Wu, Y. K. Kuo, and C. S. Lue, Phys. Rev. B **91**, 165141 (2015).
[44] C. N. Kuo, W. T. Chen, C. W. Tseng, C. J. Hsu, R. Y. Huang, F. C. Chou, Y. K. Kuo, and C. S. Lue, Phys. Rev. B **97**, 094101 (2018).
[45] E. B. Lopes, M. Almeida, and J. Dumas, Phys. Rev. B **42**, 5324 (1990).
[46] M. Falkowski, P. Doležal, A. V. Andreev, E. Duverger-Nédellec, and L. Havela, Phys. Rev. B **100**, 064103 (2019).
[47] B. Shen, F. Du, R. Li, A. Thamizhavel, M. Smidman, Z. Y. Nie, S. S. Luo, T. Le, Z. Hossain, and H. Q. Yuan, Phys. Rev. B **101**, 144501 (2020).
[48] M. Nagasawa, T. Nagasawa, K. Ichimura, and K. Nomura, Phys. B (Amsterdam, Neth.) **404**, 392 (2009).
[49] B. Becker, N. G. Patil, S. Ramakrishnan, A. A. Menovsky, G. J. Nieuwenhuys, J. A. Mydosh, M. Kohgi, and K. Iwasa, Phys. Rev. B **59**, 7266 (1999).
[50] Y.-K. Kuo, C. S. Lue, F. H. Hsu, H. H. Li, and H. D. Yang, Phys. Rev. B **64**, 125124 (2001).
[51] Y.-K. Kuo, F. H. Hsu, H. H. Li, H. L. Huang, C.W. Huang, C. S. Lue, and H. D. Yang, Phys. Rev. B **67**, 195101 (2003).
[52] D. E. Bugaris, C. D. Malliakas, F. Han, N. P. Calta, M. Sturza, M. J. Krogstad, R. Osborn, S. Rosenkranz, J. P. C. Ruff, G. Trimarchi, S. L. Bud'ko, M. Balasubramanian, D. Y. Chung, and M. G. Kanatzidis, J. Am. Chem. Soc. **139**, 4130 (2017).
[53] W. L. McMillan, Phys. Rev. B **16**, 643 (1977), and references therein.
[54] M. Tinkham, *Introduction to Superconductivity* (McGraw-Hill, New York, 1996).